21st Australasian Fluid Mechanics Conference
Adelaide, Australia
10-13 December 2018

Formation Mechanism of Internal Shear Layers in a Developing Turbulent Boundary Layer

J.H. Lee[1], M. Kozul[2], N. Hutchins[1] and J. P. Monty[1]

[1]Department of Mechanical Engineering
University of Melbourne, Victoria 3010, Australia

[2]Department of Energy and Process Engineering
Norwegian University of Science and Technology, Gløshaugen, 214, Norway

Abstract

The evolution and formation mechanism of large-scale shear layers in a turbulent boundary layer are investigated using time-resolved PIV datasets of a developing turbulent boundary layer from inception at the trip up to a friction Reynolds number of Re_τ =3000. The spatially developing boundary layer is formed on a 5m long flat plate towed through a water tank. By tracking large-scale coherent events using the time-resolved PIV datasets, it is found that there is a difference in the convection velocity between large-scale low- and high-speed motions at a given wall-height in the outer region. Further, an analysis of a sequence of instantaneous fields of streamwise velocity fluctuation reveals that strong streamwise velocity gradients in the wall-normal direction are prevalent along interfaces where low- and high-speed regions interact as they travel at a different speed. To provide an insight on how these regions are associated with the formation of shear layers in a turbulent boundary layer, we compute conditional averages of streamwise velocity fluctuation based on a strong shear layer. Our results reveal that one possible mechanism for the generation of shear layers is due to the mismatch in convection velocities between low- and high-speed regions. Interpretation of these findings is further supported by employing direct numerical simulation (DNS) of a temporally developing turbulent boundary layer [8]. DNS data also demonstrate that the interaction between large-scale low- and high-speed motions form shear layers in the logarithmic region, providing a possible formation mechanism and dynamics of shear layers within wall-bounded turbulent flows.

Introduction

In the study of wall-bounded turbulent flows, the existence and kinematics of coherent motions have been rigorously investigated to understand the role of these motions. The consistent occurrence of thin shear layers throughout a turbulent boundary layer at the interfaces between upstream high-speed regions and downstream low-speed regions has been commonly reported in the literature [11], especially in the near-wall region. Flow visualisation studies [3] suggest that there is a direct relationship between an entering high-speed region and a low-speed region near the wall, causing the ejection by a local instability mechanism (i.e. a developing oscillation). This suggests that the presence of shear layers and an associated instability can lead to the formation of a strong ejections near the wall. The shear layers are not only observed in the near wall region but also away from the wall where large-scale motions are dominant. Intense shear layers are also known to demarcate two large regions with nearly uniform streamwise momentum [1]. More recently, an interaction between ejection events (Q2 events) and an in-rushing high-speed region (Q4 event) has been observed to cause a shear layer that can deform an existing hairpin structure. The subsequent roll-up in the spanwise direction generates a new vortex closer to the wall that is observed both numerically [5] and experimentally [6]. Although many of these studies have shed new light on the existence of the shear layers, the origin, lifespan and development of these features still remain largely unresolved. Hence in the current study, we attempt to further examine the formation mechanism of the shear layers in an evolving turbulent boundary layer from an inception to a moderate Reynolds number state using a temporally resolved PIV database. These experiments take advantages of the towed-plate coupled with a stationary time-resolved PIV (TRPIV) system such that the evolving large-scale features can be tracked in time. These events appear nominally stationary within the field of view since the freestream velocity in this case is zero. Experimentally, this provides a unique database of the developing turbulent boundary layer. This frame of reference is analogous to moving an entire PIV system with the flow, tracking large-scale flow features as they advect downstream in a water channel [12].

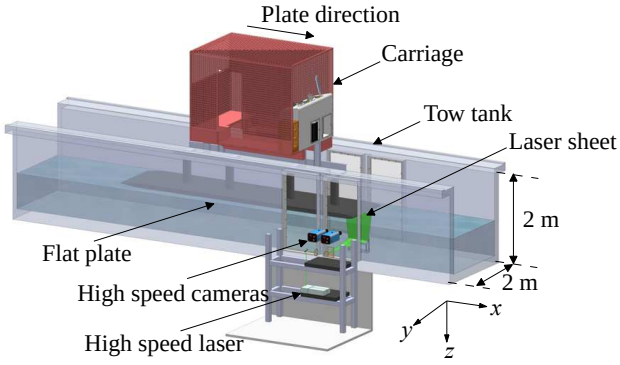

Figure 1: Time-resolved PIV setup with flat plate in tow tank

Facility and Measurement set-up

The experiments are performed in the tow tank facility located in the Michell hydrodynamics laboratory at the University of Melbourne. The tow tank has dimensions of 60 × 2 × 2 m (length × width × height) and is filled with water. As indicated in figure 1, the fully-automated traversing carriage tows a 5 m long and 1.2 m wide flat plate at a towing velocity of approximately 1.0 m/s ($U_{plate} \equiv U_\infty$ after Galilean transformation). Full details of the facility including the influence of edge effects and the carriage automation are available in [9]. A visual aid to demonstrating the entire towed plate experiment and a sequence of time-resolved instantaneous streamwise velocity fields of a developing turbulent boundary layer is available online[1]. Throughout this paper, x, y and z denote the streamwise, spanwise and wall-normal directions, with u, v and w denoting the respective fluctuating velocity components. Overbars indicate time-averaged quantities (e.g. $\overline{U}$). The superscript '+' is used to denote quantities normalised by viscous scaling for length ($z^+ = zU_\tau/\nu$) and velocities ($U^+ = U/U_\tau$).

The time-resolved PIV setup consists of a Photonics DM20-

[1]http://dx.doi.org/10.1103/APS.DFD.2014.GFM.V0054

Re_τ	δ (mm)	U_τ (ms^{-1})	l^+	Δt^+
700 - 3300	15 - 90	0.045 - 0.037	54 - 66	1.37 - 2.01

Table 1: Experimental parameters for TRPIV in the towed plate experiments. Ranges indicate the variation of parameters over the streamwise length of the plate $0 < x_{plate}$ (m) < 5 when U_{plate} = 1 m/s.

527 dual head Nd:YLF laser, and two PCO Dimax CMOS cameras with 32GB buffer that have a resolution of 2000 $\times$ 2000 pixels. The two cameras are located side-by-side providing an elongated field of view in the streamwise direction of 170 $\times$ 80 mm ($x \times z$). The laser sheet illuminates an $x-z$ plane (streamwise/wall-normal) along the centre line of the flat plate. The tank is seeded with hollow glass spheres with a mean diameter of 10 μm. All images are acquired at a sampling rate of 1000 Hz which gives Δt = 1 ms (where Δt is the time between images). This equates to $\Delta t^+ \approx 1.7$ at $U_{plate} = 1$ m/s. Experimental conditions are summarised in table 1, where x_{plate} is the streamwise distance downstream of the trip device. Both boundary layer thickness (δ) and friction velocity (U_τ) are obtained from the composite velocity profile of [2]. Further details of the development of the experimental parameters are described in [9], which also validate the integral properties of the evolving turbulent boundary layers, demonstrating that this is a well-behaved canonical turbulent boundary layer.

In order to validate the quality of the database from the current experiment, figure 2 shows viscous-scaled mean velocity and turbulence intensity profiles. The symbols and grey shade correspond to results from the TRPIV database, while the solid lines correspond to a simulation database [4]. Since the simulation database covers the range of Reynolds number obtained from the current study, the comparison between these two datasets provides a verification that the experiment is not beset by any experimental uncertainties. The results show good agreement for the mean velocity profile between the experiments and the DNS at comparable Reynolds numbers. Similarly, the turbulence intensity profiles shown in figure 2 (b,c) also exhibit good agreement with some degree of spatial attenuation, which is to be expected from PIV measurements. Hence, here we used the tool proposed in [10], which accounts for the unresolved small-scale missing energy due to limited spatial resolution in PIV experiments. The estimated attenuated turbulence intensity profiles from the DNS with spatial resolution matched to the PIV interrogation volume (including laser sheet thickness) are shown by the dashed lines. Good agreement is observed between the TRPIV and the estimation, indicating that the discrepancy in the turbulence intensity profiles is mainly due to spatial averaging.

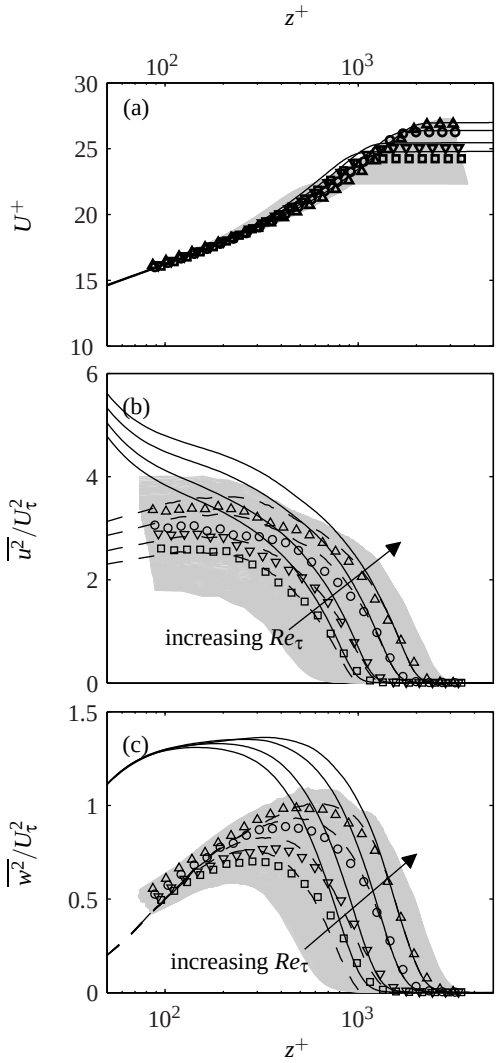

Figure 2: Inner-scaled flow statistics at various x_{plate} positions for TRPIV. A total of 462 profiles out of 4500 are plotted in gray and four profiles plotted with symbols have $Re_\tau \approx 1300$ ($\circ$), 1600 ($\triangledown$), 2000 ($\square$) and 2500 ($\triangle$). (a) Mean streamwise velocity profiles. Turbulence intensity profiles for (b) streamwise velocity and (c) wall-normal velocity components. Solid lines are reference statistics from turbulent boundary layer simulation data of [4]. Dashed lines indicate under-resolved statistics using the estimation method proposed in [10].

Results

Figures 3 (a-d) display a sequence of viscous-scaled streamwise velocity fluctuations u^+ while the plots (e-h) show the associated dU^+/dz^+ from the time-resolved PIV datasets. In figure 3(a-d), one can observe that the low-speed region (marked with an ellipse) entering from the right side of the field of view starts to interact with the adjacent high-speed region as time progresses. And the corresponding dU^+/dz^+ sequence shown in figure 3(e-h) indicates that this interaction is accompanied by the formation of a strong inclined shear layer (marked with an ellipse). Lee *et al.* [9] have previously shown that there is a difference in the convection velocity between low- and high-speed regions at a given wall height and in the frame of reference of the towed plate experiment, with the low-speed regions convecting closer to the plate velocity (faster) than the high-speed regions at a given wall-normal location. Applying a Galilean transformation allows conversion of the moving plate frame of reference to a more conventional wind tunnel frame of reference by subtracting the plate velocity. Hence, the observation from figure 3 suggests that the mismatched convection velocities between the low- and high-speed regions lead to these regions coming together or interaction which in turn will give rise to a shear layer at the interface between the two regions. This scenario may be a prominent formation mechanism of an internal shear layer in the outer region of turbulent boundary layers. In the following analysis, the detection of strong shear layers and conditional averaging are used to test this hypothesis.

The relationship between the mismatch in the convection velocity and the formation of the internal shear layer can be examined by computing spatial and temporal conditional quantities as follows. First of all, we define a strong internal shear layer as the region when the instantaneous $d\tilde{U}^+/dz^+$ is higher than the local mean $d\overline{U}^+/dz^+$ (any change in the threshold does not significantly alter the results of this pronounced instantaneous

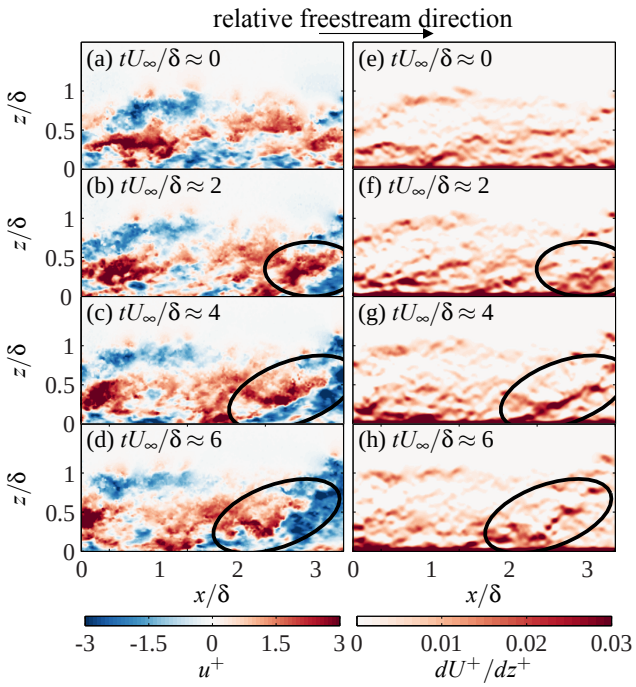

Figure 3: (a-d) sequence of the streamwise velocity fluctuation, u^+ and (e-h) the corresponding instantaneous wall-normal gradient of the streamwise velocity, dU^+/dz^+. Time separation between plots is approximately $\Delta tU_\infty/\delta \approx 2$.

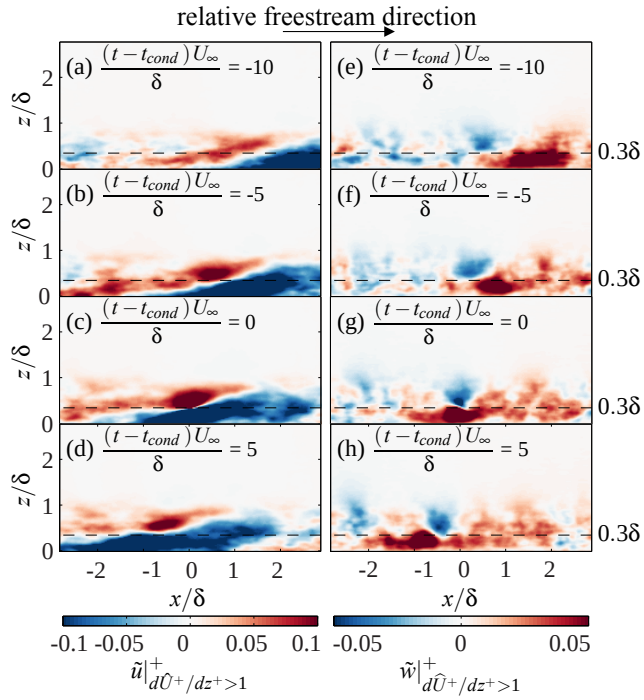

Figure 4: Iso-contours of a sequence of the conditionally averaged streamwise and wall-normal velocity fluctuation fields computed based on a strong shear layer event at $z/\delta = 0.3$ at $Re_\tau \approx 1400$. This sequence shows the prior and subsequent fields relative to the reference time. The sequence has a time step of $(t-t_{cond})U_\infty/\delta_{local} = 5$.

behaviour). Throughout the analysis, $d\tilde{U}^+/dz^+$ is normalised by $d\overline{U}^+/dz^+$ and defined as

$$d\widehat{U}^+/dz^+ \equiv (d\tilde{U}^+/dz^+)/(d\overline{U}^+/dz^+). \quad (1)$$

We can now employ a lag and lead conditional averaging scheme used by [7]. The conditional points are first selected in a region where $d\widehat{U}^+/dz^+ > 1$ at a fixed wall-height and at a given reference time (t_{cond}). Then we can ensemble a conditional sequence around (prior/after) the reference time. This will enable us to statistically monitor the spatio–temporal development of the associated motions related to the formation of the shear layers. A Gaussian filter size of $0.2\delta \times 0.1\delta$ ($x \times z$) is used on the datasets to avoid conditioning on small-scale events.

Figure 4 shows a sequence of iso-contours of conditionally averaged streamwise and wall-normal velocity fluctuations at $z/\delta = 0.30$, which occurs at $Re_\tau \approx 1400$. This sequence ranges for 15 boundary layer turnover times ($\Delta tU_\infty/\delta$) prior/after the detected event. The sequence starts with a low-speed and high-speed event within the log region separated by some distance. As the conditioned time approaches the reference time (figure 4 a-c), the low-speed region catches up with the high-speed region (due to their different convection velocity), and this interaction seems to force the high speed region further from the wall. At the reference time (shown in figure 4 c), it can be seen that the low-speed region collides with the high-speed region from below, giving rise to an inclined internal shear layer extends deep into the logarithmic region. Similar conditional sequences are observed over a Reynolds number range $1000 < Re_\tau < 3000$ (not shown here for brevity). The right column of figure 4 shows the iso-contours of the conditionally averaged sequence of w fluctuations. It is interesting to note that during the formation of the strong internal shear layers, the positive w fluctuations are highly correlated with the low-speed region and vice versa. This indicates that an instantaneous strong shear forms in the outer region when a low-speed region, characterised by flow away from the wall, interacts with a high-speed region, which is directed towards the wall. The sequence of instantaneous u fluctuations fields shown in figure 3 shows comparable events to the ensemble averaged fields conditioned upon the strong internal shear layer. Therefore, the persistent appearance of the interaction between the low- and high-speed regions due to the mismatch in the convection velocities in both instantaneous and ensemble-averaged fields suggests that it could be considered as a formation mechanism of the strong internal shear layers witnessed in the outer region. It is worth stressing that we are here only able to analyse a two-dimensional streamwise-wall-normal slice through what is likely to be a complex three-dimensional structure. Temporally resolved DNS fields of an evolving turbulent boundary layer are necessary to show a detailed view of the three-dimensional structure. Hence, we employ temporally developing turbulent boundary layer DNS datasets with Reynolds number in the range $300 \lesssim Re_\tau \lesssim 800$ [8], which also have the moving wall frame of reference to further investigate the shear layer formation mechanism in a three-dimensional aspect.

Figure 5 shows instantaneous u^+ and dU^+/dz^+ in a $x-z$ plane and instantaneous u^+ and v^+ in a $x-y$ plane at various wall-normal locations sliced from the DNS. The dashed lines on the $x-z$ plane plot indicate the wall-height locations of the various wall-parallel plane views. Similar to the results from the plate PIV (shown in figure 3), a strong shear layer is observed along the interface where the low- and high-speed regions interact. In the wall-parallel ($x-y$) plane, there is a clear collision between these two regions (marked with an ellipse) not only in the outer region but also within the logarithmic region ($z/\delta \sim 0.1$). The dashed lines indicate the location where the $x-z$ plane is extracted. The associated spanwise motion at the onset of the interaction is demonstrated in the wall-parallel plots of v^+. The plots reveal a strong lateral motion ($\pm v^+$) within the region coincides with the location where the low- and high-speed regions interact. The fact that there is a strong spanwise motion at the interface between the low- and high-speed regions

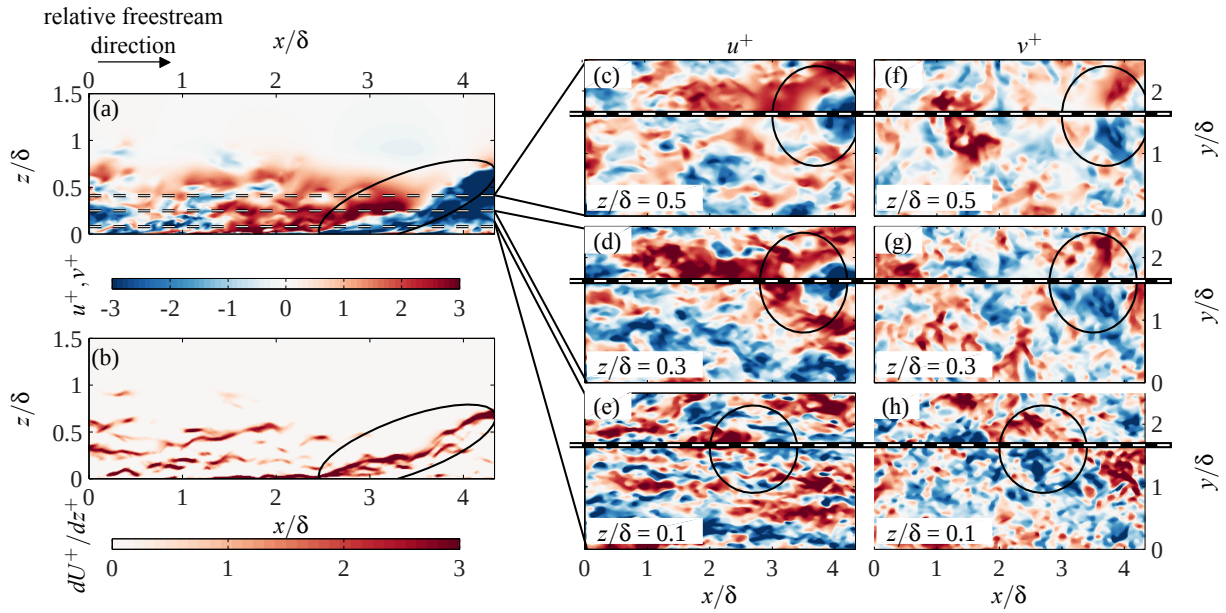

Figure 5: Instantaneous flow fields from developing turbulent boundary layer simulation ($300 \lesssim Re_\tau \lesssim 800$) [8]. (a) u^+ and (b) dU^+/dz^+ are shown in $x-z$ plane and wall-parallel plane of corresponding (c-e) u^+ and (f-h) v^+ at $z/\delta = 0.1$, 0.3 and 0.5. The dashed lines on (a) shows the wall height locations of $x-y$ plane plots and the dashed lines on (c-h) indicate the corresponding spanwise location of $x-z$ plane plots. Ellipses indicate region where $+u$ and $-u$ interacts.

could indicate that the meandering of large-scale motions might be influenced by a series of interaction between these low- and high-speed regions within the turbulent boundary layers. These observations from the DNS data, together with the conditional time sequence from the PIV fields provide evidence that one possible mechanism for the generation of internal shear layers is an interaction between low- and high-speed regions due to the mismatch in the convection velocities.

Conclusions

Time-resolved PIV of a towed plate is used to investigate the evolution of turbulent boundary layers from an inception to a moderate Reynolds number state. A formation mechanism of internal shear layers and dynamical characteristics of associated large-scale coherent motions are investigated using the temporally resolved spatial datasets. The resulting lag and lead conditional averages reveal that the mismatch in the convection velocity between low- and high-speed regions at a given wall height allows these regions to catch up to each other, causing an interaction that is associated with shear layer formation. Three-dimensional view of this shear layer formation from a complementary DNS database further confirms that a large-scale shear layer is observed along interfaces where these two different regions interact not only in the outer region but also within the logarithmic region, and it is noted that such interactions are accompanied by a strong spanwise motion. These spanwise motions and associated shear layers may be related to the meandering of large-scale flow motions. Further investigation is required to confirm whether this conjecture is statistically observed.

Acknowledgements

The authors gratefully acknowledge the financial support of the Australian Research Council.

References

[1] Adrian, R. J., Meinhart, C. D. and Tomkins, C. D., Vortex organization in the outer region of the turbulent boundary layer, *Journal of Fluid Mechanics*, **422**, 2000, 1–54.

[2] Chauhan, K. A., Monkewitz, P. A. and Nagib, H. M., Criteria for assessing experiments in zero pressure gradient boundary layers., *Fluid Dynamics Research*, **41**, 2009, 021404.

[3] Corino, E. R. and Brodkey, R. S., A visual investigation of the wall region in turbulent flow, *Journal of Fluid Mechanics*, **37**, 1969, 1–30.

[4] Eitel-Amor, G., Örlü, R. and Schlatter, P., Simulation and validation of a spatially evolving turbulent boundary layer up to $Re_\theta = 8300$, *International Journal of Heat and Fluid Flow*, **47**, 2014, 57–69.

[5] Goudar, M. V., Breugem, W. P. and Elsinga, G. E., Auto-generation in wall turbulence by the interaction of weak eddies, *Physics of Fluids*, **28**, 2016, 035111.

[6] Jodai, Y. and Elsinga, G. E., Experimental observation of hairpin auto-generation events in a turbulent boundary layer, *Journal of Fluid Mechanics*, **795**, 2016, 611–633.

[7] Johansson, A. V., Alfredsson, P. H. and Kim, J., Evolution and dynamics of shear-layer structures in near-wall turbulence, *Journal of Fluid Mechanics*, **224**, 1991, 579–599.

[8] Kozul, M., Chung, D. and Monty, J. P., Direct numerical simulation of the incompressible temporally developing turbulent boundary layer, *Journal of Fluid Mechanics*, **796**, 2016, 437–472.

[9] Lee, J. H., *Evolution of canonical turbulent boundary layers*, Ph.D. thesis, The University of Melbourne, 2017.

[10] Lee, J. H., Kevin, Monty, J. P. and Hutchins, N., Validating under-resolved turbulence intensities for PIV experiments in canonical wall-bounded turbulence, *Experiments in Fluids*, **57**, 2016, 129.

[11] Robinson, S., Coherent motions in the turbulent boundary layer, *Annu. Rev. Fluid Mech.*, **23**, 1991, 601–639.

[12] Zheng, S. and Longmire, E. K., Perturbing vortex packets in a turbulent boundary layer, *Journal of Fluid Mechanics*, **748**, 2014, 3683–398.